

Computational Geometry Solution to Nonunique Forward Model Inversion for Multi-ink Printing

Gustav J. Braun, Kevin E. Spaulding, John D'Errico, and Douglas W. Couwenhoven, Eastman Kodak Company, Rochester, NY/USA

Abstract

Forward device models for multi-ink printing systems (i.e., ones that contain more than three colorants) relate ink amounts to predictions of either colorimetry or spectral reflectance. These models often have a large portion of their range (CIELAB values) that lack unique domain values (device ink amounts). This makes unique inversion of the forward model ill posed in these regions of color space. An approach is presented where direct computational techniques are applied to a tessellated version of a device's forward model to produce an inverse. This is accomplished using an isosurfacing technique that sequentially intersects m noncoincident planes in the m -dimensional range color space through the image of the model's device-code value n -dimensional domain tessellation. This computational approach results in $(n-m)$ -dimensional piecewise-linear ink manifolds that define the mapping of the n -dimensional domain space (ink amounts) to a location in the m -dimensional range space (CIELAB). This process is generalizable to devices with any number of input inks, $n \geq m$, provided the range space color is within the color gamut of the device.

Keywords: Device modeling, forward model inversion, color management, profiles.

Background

Colorimetric or spectral forward models of an imaging device relate the device code values or colorant amounts to either direct colorimetric quantities, such as tristimulus values, or to spectral quantities, as is the case of Yule-Nielson modified spectral Neugebauer models [1]. For color management purposes, the inverse of these models is required (i.e., the relationship between device-independent color values, such as CIELAB values, and device code values). The process of inverting these device models is the key to modern color management.

For well-behaved three-color imaging devices, such as *RGB* displays and *CMY* printers, the relationship between device code values and colorimetric quantities, such as CIE tristimulus values or CIELAB values, is unique. This relationship is shown diagrammatically for an *RGB* display in Fig. 1. In this figure, the device code values span a cube of red, green, and blue domain values and the color gamut spans a region of the CIELAB range space. The example shown in Fig. 1 uses a tetrahedral complex (i.e., a connected group of tetrahedral simplexes) to represent the forward device model. Forward models of this type have the relationship that each vertex in the domain space has a matching point in the range space and the connectivity of the tetrahedral complex (i.e., which vertices belong to which tetrahedron) is the same in both the domain and range spaces. Inversion techniques

based on tetrahedral interpolation for unique forward models can be found in Hung [2].

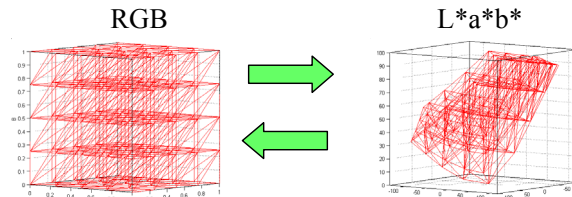


Figure 1. Three-dimensional forward and inverse model.

For printing or display systems that use more than three colorants or primaries, a dimension mismatch between the domain space (the *CMYK* colorants) and the range space (CIELAB) exists. The dimensionality mismatch between the colorant domain and the color domain make direct inversion of a model or simplicial complex ill posed. Forward model inversions for four-color *CMYK* systems usually rely on dimensional constraints such as under-color removal (UCR) techniques that control the use of the black ink in the input domain [3]. By constraining the behavior of the black ink functionally to the C, M, and Y inks, the effective dimensionality of the input domain is reduced to the number of freely varying colorants (in this case, three). Other forms of dimensional constraint have been achieved by partitioning the forward model into multiple subspaces of a fixed amount of one of the colorants (e.g., black ink) [4]. For each subspace, there is a unique forward model that spans a portion of the device's full gamut. Thus, for any value of the constrained color, an inverse solution is available provided the target color is within a particular subspace. By performing model inversions for multiple values of the black ink, a set of colorant domain values can be built. Points in this set lie on an ink manifold in the colorant domain. Selection of the optimal value can then be made based on a cost function.

While both the UCR approach and the input domain partitioning approach offer successful techniques for reducing the dimensionality of four-color forward devices, they suffer extensibility issues as the dimensionality of the input domain increases. For example, consider the case of a six-color printing system that uses cyan, magenta, yellow, black, orange, and green colorants. For this six-ink printer, the six-dimensional input domain can be tessellated to form a simplicial complex of 6-plexes (i.e., simplexes with seven vertices that reside in the six-dimensional input domain) using a Delaunay tessellation process [5]. The range space values of these colorant mixtures can be estimated by using a physical model, direct measurement, or curve-fitting and interpolation techniques.

For the case of *CMYK* printing systems, the dimensional mismatch between the colorant domain and the CIELAB range space is one—four dimensions from the *CMYK* colorant space minus three dimensions from the CIELAB color space. As such, only one colorant needs to be constrained to overcome this dimensional mismatch. For the six-color printer, the dimensional mismatch between the colorant domain and the color space range is three. It follows that three of the colorants would need to be fixed in order to create a dimensional match with the CIELAB range space.

Boll defined a partitioning scheme whereby a seven-color printer (*CMYKRGB*) was partitioned into six four-color models where each submodel consisted of three chromatic colorants and a black [6]. By adopting a UCR strategy for each of the four-color models, he was able to invert the models in a manner similar to those described above. Boll also generated inking rules to handle the case where a given CIELAB point fell in more than one of the six subspaces. These rules had factors that included total ink amount; desire to maximize a dominant ink; and vertex-to-vertex correlation of ink amounts in the final color table, among others.

Another multi-ink inverse case was presented by Chen et al. [7] for inversion of a six-ink Yule-Nielson spectral Neugebauer model, which involved finely sampling the six-ink forward model and searching for candidate inverses that minimized a color-inconstancy index within small regions of the CIELAB color space. One limitation with this process is that there is no guarantee that the selected point has the minimum color-inconstancy properties of the input domain at that colorimetric value.

These techniques focus on reducing the dimensional mismatch between the colorant and color spaces so that unique inverses are possible, albeit within a given subdomain. The technique described in this paper solves for all domain space inverses for a given range space point for forward models of arbitrary dimension. This general inverse solution is represented as a piecewise linear approximation to a continuous manifold that defines the mapping from a CIELAB range space value to the n -dimensional input colorant domain.

Ink Manifolds

Within this manuscript, *ink manifolds* are defined as the connected set of colorant domain space points that map to a given CIELAB range space point. Mathematically this relationship can be visualized using the function shown in Fig. 2. Suppose the plot shown in Fig. 2(a) represents the two-dimensional input domain of colorants x_1 and x_2 . This input colorant domain is spanned by a complex of 2-plexes (triangles) to form a colorant domain tessellation. Consider the case where the colorant domain is related to some one-dimensional color space range value z by $z = x_1^2 + x_2^2$, Fig. 2(b). (A physical example might be where $z =$ lightness and x_1 and x_2 represent two black inks.)

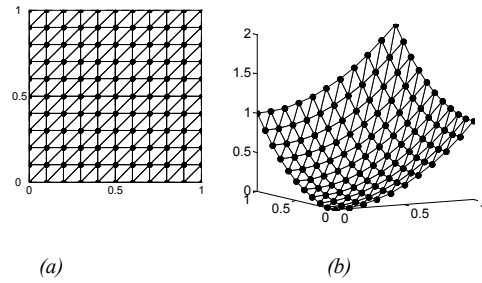


Figure 2. (a) Illustration of a two-dimensional simplicial complex of the x_1, x_2 domain. (b) Image of two-dimensional simplicial complex of the x_1, x_2 domain in the $z = x_1^2 + x_2^2$ range space.

For any value of z , there may be multiple x_1, x_2 colorant combinations. The set of x_1, x_2 colorant values that map to a given z value can be approximated by determining where the edges of the domain space tessellation cross the given z value. Pictorially, this relationship is shown for $z = 0.8$ in Fig. 3(a). In this example, a plane of constant z values is shown intersecting the triangulation surface at $z = 0.8$. The points on the surface triangulation that cross the level z value of 0.8 are input domain points on a 1-manifold of the x_1, x_2 colorant domain that map to the range space color value of $z = 0.8$. This 1-manifold is shown in the x_1, x_2 colorant domain space in Fig. 3(b) as a piece-wise linear curve. Thus, any point on this manifold is a candidate inverse for the color space value of $z = 0.8$.

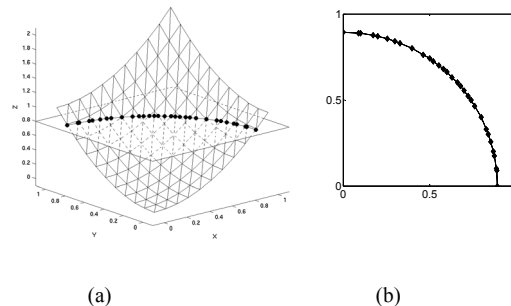


Figure 3. (a) Intersection of the image of the x_1, x_2 colorant domain tessellation with the range space level value of $z = 0.8$. (b) Diamonds are the locations of the edges of the input tessellation that intersect the level value of 0.8 in the range space. The line segments connecting these vertices represent the piecewise linear approximation to the $z = 0.8$ manifold.

Model Inversion

For the *CMYK* colorant case, the set of input domain simplexes are neither triangles (2-plexes) nor tetrahedrons (3-plexes), as was the case for the two- or three-colorant cases previously discussed, but are 4-plexes (i.e., simplexes with five vertices). The set of 4-plexes that span the full *CMYK* input domain are exactly analogous to the set of tetrahedrons that span the *RGB* domain shown in Fig. 1. A relationship of input domain *CMYK* vertices and CIELAB color values can be obtained using a physical device model, by direct colorimetric measurement, or by computational estimation using a multidimensional fitting process. For all of these cases, it is possible to estimate the CIELAB color

space value for each vertex in the *CMYK* domain space simplicial complex using the forward model.

The manifold building process (inverse modeling) shown in Figs. 2 and 3 is extensible to forward models that convert from an n -dimensional colorant domain to an m -dimensional color range where $n \geq m$. For most cases, the m -dimensional color space has three dimensions such as those for CIELAB. Two additional forward-model inversion examples build on the two-colorant inversion shown in Figs. 2 and 3 are: (1) Three-dimensional input domain mapped to three-dimensional output range results in a 0-manifold; (2) Four-dimensional input domain mapped to three-dimensional output range results in a 1-manifold.

Three-to-three Case

For the first case, consider the *RGB* forward model shown in Fig. 1, and model inversion for the color space point $L^*a^*b^* = [50\ 0\ 0]$. A level value of $L^* = 50$ can be generated by slicing through the CIELAB tessellation parallel to the a^*, b^* plane. This cutting plane intersects the edges of some of the tetrahedrons in the gamut, Fig. 4(a,b). Predictions of the *RGB* domain space code values for these intersection points are made using a linear interpolation scheme that utilizes barycentric edge weights calculated along the edges of the tetrahedron where a given intersection occurred. These barycentric edge weights are applied to the domain space code values of the tetrahedron that intersected the $L^* = 50$ plane. The domain space values are calculated for the intersection points for all tetrahedrons that intersect the $L^* = 50$ plane. These points all lie on the $L^* = 50$ 2-manifold in *RGB* code value domain. This surface is shown in Fig. 4(c).

A second slice through the $L^* = 50$ tessellation at $a^* = 0$ isolates the domain-space 1-manifold to points that map to CIELAB points with $a^* = 0$ and $L^* = 50$, and whose b^* values span the color gamut, Fig. 4(d-f). To fully isolate the CIELAB point requires that a third cutting plane at a level of $b^* = 0$ intersect the $L^* = 50$ and $a^* = 0$ CIELAB tessellation, shown in Fig. 4(g). The result of this third cutting plane is a 0-manifold (a single point) in the *RGB* domain space of point $L^*a^*b^* = [50\ 0\ 0]$. For this example, the final manifold is a 0-manifold because the range and domain spaces were both three-dimensional.

Four-to-three Case

For input domains with more than three colorants, it is impossible to visualize the domain space tessellation and the manifolds. This limitation does not impact the effectiveness of the computational method. While the input domain tessellation can no longer be visualized, the *image* of the tessellation is visible in the CIELAB range space, as shown for a single simplex of a *CMYK* tessellation in Fig. 5(a). This simplex has five vertices and eleven edges. The complete forward model is composed of a complex of similarly shaped simplexes that span the device's color gamut. In order to isolate a single CIELAB value and its inverse domain space 1-manifold, three noncoincident cutting planes are intersected with the *image* of the domain space complex.

Consider the inverse for a CIELAB point of $[95\ 1\ 1]$. For one simplex, these stages are shown in Fig. 5(b-f). A level value is first computed for a value of $L^* = 95$ and results in four intersection points ($e1, e2, e3, e4$), Fig. 5(b). A tessellation of these points is obtained by rotating them into a full rank subspace using a QR factorization [8] (Golub and Van Loan) and applying a Delaunay tessellation operation, to produce the tessellation shown in Fig. 5(c). A second cutting plane is intersected with this tessellation at a desired a^* value and results in three intersection points ($e5, e6, e7$) at constant a^* and L^* values, Fig. 5(d). A tessellation of these points is given by another QR rotation and Delaunay tessellation process resulting in the tessellation shown in Fig. 5(e). A third and final cutting plane is intersected with this tessellation at the desired b^* value to isolate the CIELAB point and produce the domain space solution to the inverse forward model for that simplex. This process is repeated for all simplexes in the *CMYK* domain space complex to produce the complete 1-manifold of *CMYK* code values that map to the specified CIELAB point.

The interpolation scheme used to estimate the colorant domain values for the intersection points is shown in Fig. 6. The *CMYK* values for point $e1$ shown in Fig. 5(b) are estimated from the *CMYK* values of the vertices $v1$ and $v2$ of the given simplex being evaluated, using barycentric weights $w1$ and $w2$. These weights are given by the fractional CIELAB distances between the vertices and the intersection point $e1$. This interpolation is repeated for each intersection point at each stage of the isolation process.

In general, the model inversion process for this technique results in domain space manifolds that are three dimensions fewer than the number of colorants. As such, three-ink systems result in a 0-manifold or a unique inverse; four-ink systems result in a 1-manifold or a piecewise linear curve in the input domain; five-ink systems result in 2-manifolds or piecewise linear surfaces in the input domain. Therefore, a colorant selection process is needed to evaluate the usefulness of the manifold points in a color transform. While a general rule for searching these manifolds is beyond the scope of this discussion, a reasonable starting point would be to consider the vertices of these manifolds as points to screen.

Sample Calculations

Because it is not possible to visualize the colorant domain manifold surfaces for domains higher than three dimensions, tabulated examples are given instead. Consider the inverse model calculation of a *CMYK* printer for a CIELAB value of $[50\ 0\ 0]$. The forward model consists of a *CMYK* domain tessellation of a 3^4 lattice of *CMYK* values (81 vertices) and 384 4-plexes. Note: a very sparse *CMYK* tessellation has been chosen so that a complete table of the inverses can be given. More populated forward models may result in hundreds of points in the final manifolds. The data shown in Table 1 give the CIELAB statistics of the vertices of the forward model. For these data, it can be seen that the *CMYK* gamut spans a large region of the CIELAB range.

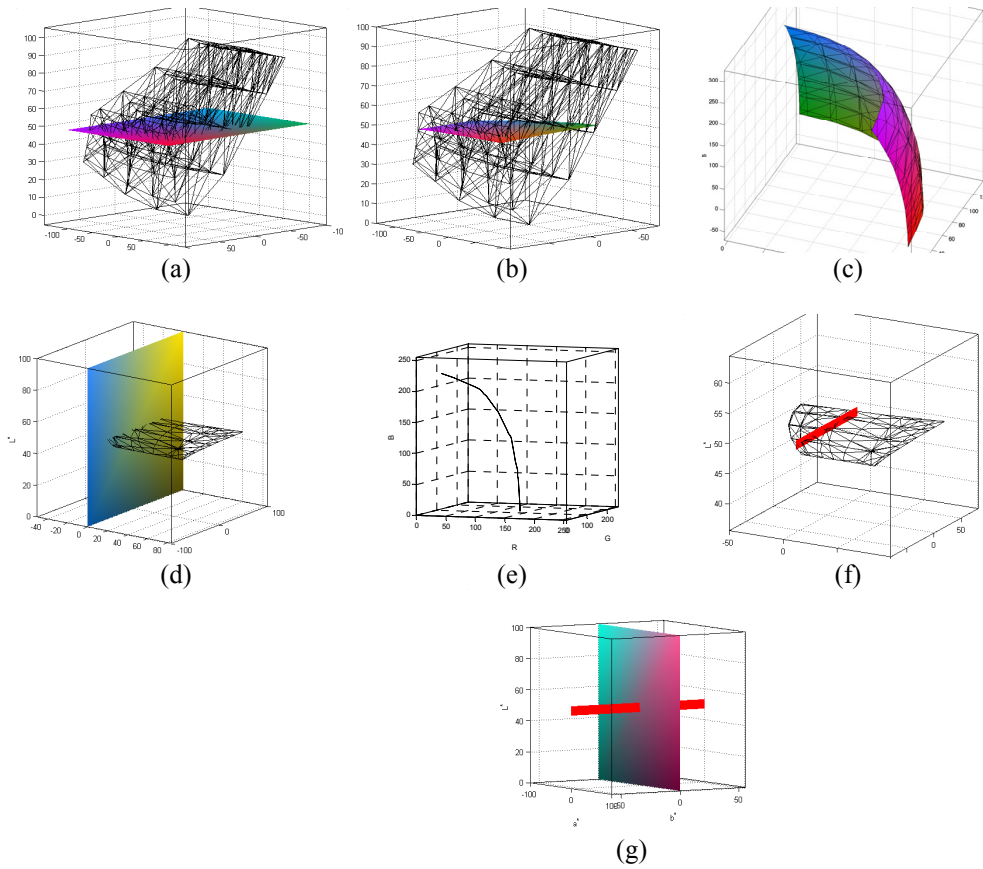


Figure 4. Isosurfacing process through the image of an RGB complex for [50 0 0] CIELAB point.

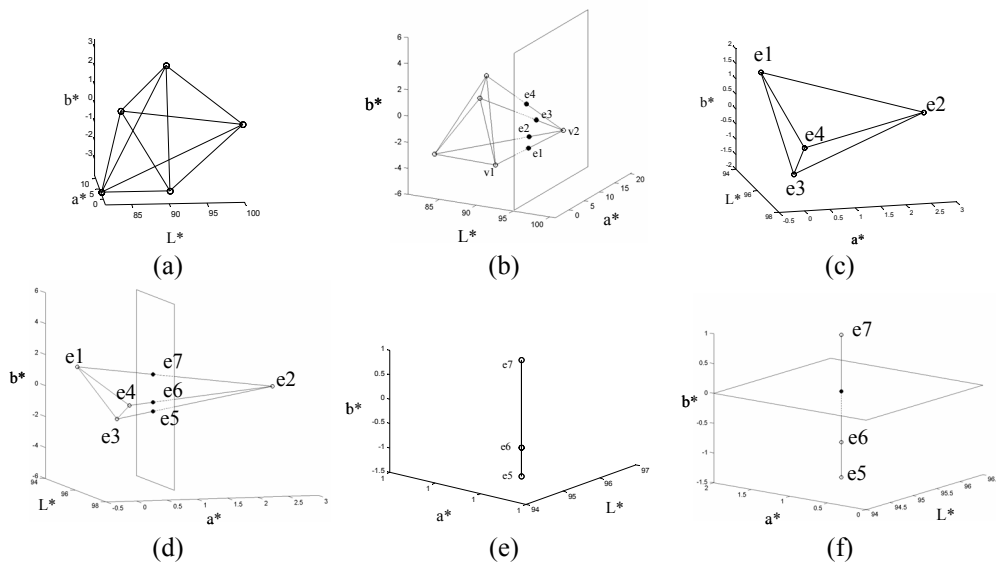


Figure 5. Isosurfacing process through image of a single simplex for a CMYK printer.

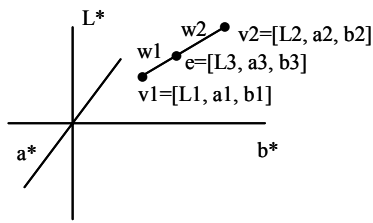


Figure 6. Linear interpolation scheme for edge intersections. Barycentric weights w_1 and w_2 are linear distance weights between points e , v_1 , and v_2 .

Slicing through the image (the CIELAB edges of the *CMYK* tessellation) at a level value of $L^* = 50$ results in 129 edge intersections. The statistics of these points are shown in Table 2. The L^* dimension is fixed at 50 while the a^* and b^* dimensions vary within the span of the gamut at $L^* = 50$. The second and third slices through the L^* tessellation result in new tessellations whose vertex values are given in Tables 3 and 4. The final manifold, represented in Table 5, consists of 24 *CMYK* points that all map to $L^*a^*b^* = [50\ 0\ 0]$ for the given 3^4 tessellation of the device's forward model.

The vertices of the 1-manifold in the *CMYK* domain are shown in Table 5. Intuitively, these values span *CMYK* combinations that use a lot of black ink (as shown in the first row) more so than those that use only *CMY* inks (as shown in the last row). To complete the forward model inversion, a point from this 1-manifold would be selected using some goodness criteria such as minimum color inconstancy value, minimum total colorant amount, minimum halftone noise, etc. This selection process is very application specific and beyond the scope of this discussion.

Table 1. CIELAB statistics of the *image* of the *CMYK* complex

	L^*	a^*	b^*
Min	2.8	-105.2	-71.2
Max	93.9	78.7	95.4
Mean	28.2	-2.4	0.1
Std	23.1	31.4	28.5

Table 2. CIELAB statistics of tessellation after $L^*=50$ slice

	L^*	a^*	b^*
Min	50.0	-94.3	-59.7
Max	50.0	72.2	59.2
Mean	50.0	-0.4	3.2
Std	0.0	29.4	29.3

Table 3. CIELAB statistics of tessellation after $L^*=50$ and $a^*=0$ slices

	L^*	a^*	b^*
Min	50.0	0.0	-47.7
Max	50.0	0.0	55.8
Mean	50.0	0.0	0.7
Std	0.0	0.0	24.3

Table 4. CIELAB statistics of tessellation after $L^*=50$, $a^*=0$, $b^*=0$ slices

	L^*	a^*	b^*
Min	50.0	0.0	0.0
Max	50.0	0.0	0.0
Mean	50.0	0.0	0.0
Std	0.0	0.0	0.0

Table 5. *CMYK* code values for $L^*a^*b^*=[50\ 0\ 0]$ 1-manifold

	C	M	Y	K	L^*	a^*	b^*
0.00	0.02	0.06	0.52	50	0	0	
0.01	0.02	0.06	0.51	50	0	0	
0.02	0.03	0.08	0.50	50	0	0	
0.07	0.08	0.13	0.47	50	0	0	
0.16	0.18	0.23	0.42	50	0	0	
0.21	0.23	0.28	0.39	50	0	0	
0.25	0.27	0.32	0.37	50	0	0	
0.28	0.30	0.35	0.35	50	0	0	
0.31	0.34	0.36	0.34	50	0	0	
0.32	0.34	0.36	0.33	50	0	0	
0.33	0.34	0.37	0.33	50	0	0	
0.43	0.46	0.50	0.12	50	0	0	
0.44	0.47	0.52	0.11	50	0	0	
0.45	0.47	0.53	0.10	50	0	0	
0.45	0.47	0.54	0.09	50	0	0	
0.46	0.49	0.57	0.07	50	0	0	
0.48	0.50	0.57	0.04	50	0	0	
0.49	0.52	0.57	0.03	50	0	0	
0.49	0.52	0.57	0.02	50	0	0	
0.49	0.52	0.57	0.02	50	0	0	
0.50	0.53	0.57	0.01	50	0	0	
0.50	0.53	0.57	0.01	50	0	0	
0.50	0.53	0.57	0.01	50	0	0	
0.50	0.53	0.57	0.00	50	0	0	

Conclusions

A process for calculating the inverse to a nonunique forward device model was given. This process uses computational geometry techniques borrowed from level set theory to create inverse device models in the form of piecewise linear manifolds for given CIELAB color space values. Colorimetric inverses are possible using this technique for imaging systems with any number of colorants higher than two.

References

- [1] L.A. Taplin and R.S. Berns, Spectral Color Reproduction Based on a Six-Color Inkjet Output System, IS&T/SID Ninth Color Imaging Conference, 209-213 (2001).
- [2] P.C. Hung, Colorimetric Calibration in Electronic Imaging Devices using a Look-up-table Model and Interpolations, J. Electron. Imaging 2(1), 53-61 (1993).
- [3] R. Bala, Inverse Problems in Color Device Characterization, Proceedings of the SPIE, 5016, 185-195 (2003).
- [4] K.E. Spaulding, D.W. Couwenhoven, and R.L. Miller, Method and Apparatus for Calibrating a Four Color Printer, US Patent 5,553,199.
- [5] J.E. Goodman and J. O'Rourke, eds., Handbook of Discrete and Computational Geometry (CRC Press, New York, 1997) pp. 377-388.
- [6] H.A. Boll, Color to Colorant Transformation for a Seven Ink Process, IS&T/SPIE Symposium on Electronic Imaging, Science and Technology, 6-10 February (1994).
- [7] Y. Chen, R.S. Berns, L.A. Taplin, and F.H. Imai, A Multi-ink Color-Separation Algorithm Maximizing Color Constancy, IS&T/SID Eleventh Color Imaging Conference, 277- 281 (2003).
- [8] G.H. Golub and C.F. Van Loan, Matrix Computations, 3rd edition (Johns Hopkins University Press, Baltimore, MD, 1996) pp. 223-236.

Biography

Gustav Braun is a Senior Principal Scientist in the Inkjet Systems Division at Eastman Kodak Company. He received his Ph.D. in Imaging Science from the Center for Imaging Science at the Rochester Institute of Technology in 1999. His current research interests include digital color reproduction, color gamut mapping, digital printing, and device modeling.